Chemical Engineering Journal 545 (2026) 179623

Contents lists available at ScienceDirect

Chemical Engineering Journal

journal homepage: www.elsevier.com/locate/cej

Brush polyelectrolyte complex with high bacterial binding efficiency and biofilm penetration to efficiently prevent and treat biofilm-associated infections

Yu Liu [a], Jin Shi [a], Peng Wang [a], Zhiyong Liu [a], Tingting Cao [b], Dengwei Yu [a], Jingrui Shen [a], Lichen Yin [a], Jianjun Cheng [b,c,d,*], Haoyu Tang [a,**]

[a] Institute of Functional Nano & Soft Materials (FUNSOM), Collaborative Innovation Center of Suzhou Nano Science and Technology, Soochow University, Suzhou, Jiangsu, 215123, China
[b] Department of Materials Science and Engineering, Westlake University, Hangzhou, Zhejiang, 310030, China
[c] Research Center for Industries of the Future, Westlake University, Hangzhou, Zhejiang, 310030, China
[d] Institute of Advanced Technology, Westlake Institute for Advanced Study, Hangzhou, Zhejiang, 310024, China

ARTICLE INFO

Keywords:
Polyelectrolyte complex
Biofilm-associated infection
Bacterial binding efficiency
Biofilm penetration
Brush polyelectrolyte

ABSTRACT

Biofilm-associated infections on medical implants pose significant clinical challenges. This study reports a biofilm inhibition and eradication brush polyelectrolyte (HA-K) composed of a hyaluronic acid backbone and poly($_L$-lysine) side chains. HA-K self-assembles into a uniform polyelectrolyte complex (PEC, 300–400 nm) driven by electrostatic, hydrophobic, and hydrogen-bonding interactions. This brush polyelectrolyte complex possesses promising stability against pH (3.5–9.5) and concentration (up to 100 mg/mL) variations. It achieves exceptional biofilm inhibition efficacy (> 97.8% for *S. aureus*, > 99.9% for *E. coli*) without inducing drug resistance. Mechanistically, HA-K PEC displays >80% binding efficiency toward planktonic bacteria, potently inhibiting bacterial binding with both implant surfaces and epithelial cells. Meanwhile, HA-K PEC can efficiently penetrate mature biofilms (e.g., 5-day-old) by dissociation into small nanoparticles (50–100 nm) and destruction of biofilm extracellular polymeric substances. Besides, HA-K PEC enhances bacterial twitching motility, increases ROS production and membrane permeability within biofilms, leading to efficient biofilm eradication. In vivo studies reveal that HA-K PEC prevents bacterial colonization on implants and alleviate biofilm-associated infections/inflammation. HA-K PEC also displays negligible cytotoxicity/hemolysis and can be readily metabolized by the liver and kidney within 48 h. This work presents an efficient strategy to combat biofilm-associated infections by simultaneously preventing and treating bacterial biofilms while minimizing the risk of drug resistance.

1. Introduction

The colonization of bacterial biofilms on the surfaces of organs, tissues, and implantable medical devices presents a significant challenge in the prevention and treatment of clinical infections. Mature biofilms, protected by a physical barrier formed by extracellular polymeric substances (EPS) and bacterial dormancy [1,2], can resist antibiotic penetration and induce persistent infections [3–5], leading to chronic disease (e.g., non-healing wounds) in up to 80% of cases [6,7]. While traditional bactericidal strategies (e.g., antibiotics) can temporarily inhibit planktonic bacteria, they accelerate the accumulation of dead bacteria and exacerbate the global drug resistance crisis [8,9]. Moreover, invasive procedures such as surgical debridement can cause secondary injury [10,11]. Non-bactericidal strategies, such as using bacterial adhesion inhibitors and antifouling coatings, have emerged to reduce the risk of drug resistance [12–15]. However, they often fail to completely prevent bacterial adhesion and biofilm formation and lack the biofilm-eradicating capability needed to effectively combat biofilm-associated infections.

Polyelectrolyte complexes (PECs) are a promising class of biomaterials that have been extensively explored as drug delivery carriers, surface coatings, and more [16,17]. By combining oppositely charged polyelectrolytes, PECs with tunable structures (e.g., nanoparticles and layer-by-layer self-assembled films) and functions (e.g., antifouling and

* Correspondence to: J. Cheng, Department of Materials Science and Engineering, Westlake University, Hangzhou, Zhejiang, 310030, China.
** Corresponding author.
E-mail addresses: chengjianjun@westlake.edu.cn (J. Cheng), hytang@suda.edu.cn (H. Tang).

https://doi.org/10.1016/j.cej.2026.179623
Received 5 April 2026; Received in revised form 14 July 2026; Accepted 16 July 2026
Available online 17 July 2026

antibacterial) can be readily fabricated [18–21]. In terms of combating biofilm-associated infections, PECs have been used as delivery carriers of antibiotics and other antibacterial reagents to enhance biofilm penetration [22–24]. However, bacterial drug resistance can inevitably occur when trace antibiotics are exposed to bacteria via an uncontrolled release. Complicated fabrication processes, such as layer-by-layer self-assembly, are time-consuming and require additional equipment. The stability of PECs in aqueous solutions is another concern that PECs frequently undergo liquid-liquid phase separation (LLPS) under pH or concentration variations [25,26]. Some layer-by-layer self-assemble PEC coatings have displayed antibacterial and antifouling dual functions to prevent biofilm formation on implant surfaces [27,28]. Yet, poor antibacterial activity and dissociation of the PEC coatings eventually result in biofilm-associated infections [29]. Overall, PEC based materials have shown interesting biofilm penetration and antibacterial properties. However, the stability of PECs still requires improvement, and PECs designed solely for the prevention and treatment of bacterial biofilms have not yet been developed.

We designed a brush polyelectrolyte (HA-K, Fig. 1) by covalent integration of anionic hyaluronic acid (HA, as backbone) and cationic poly($_L$-lysine) (as side-chain). HA-K can self-assemble into PEC nanoparticles exclusively. HA-K PEC is different from conventional PEC nanoparticles that are generally prepared by self-assembling cationic polymers (e.g., antibacterial polymers) and anionic polymers. Conventional PEC nanoparticles have suffered from complicated fabrication processes and stability issues [30]. In comparison, HA-K PEC can be simply prepared by directly dissolving in aqueous solutions. The brush-like architecture of HA-K is composed of covalently linked cationic and anionic segments. It improves the stability of HA-K PEC against dissociation and binding affinity for planktonic bacteria via multivalent interactions, including electrostatic interactions, hydrophobic interactions, hydrogen bonding interactions, and so on. This work provides the first example of exclusive PECs with superior biofilm inhibition and eradication properties without raising any drug resistance. The underlying mechanisms have been investigated. The biosafety and in vivo antibacterial adhesion and antibiofilm properties of HA-K PEC suggest its potential to prevent and treat biofilm-associated infections.

2. Results and discussion

2.1. Synthesis and characterization of HA-K

Poly(*N*ε-tert-butylcarbonyl-$_L$-lysine) (BK) with amino end groups was first synthesized via a ring-opening polymerization (ROP) of *N*ε-tert-butylcarbonyl-$_L$-lysine *N*-carboxyhydrides (BLL-NCA), using *n*-butylamine as the initiator and *N,N*-dimethylformamide (DMF) as the solvent. Amidation reaction between BK and hyaluronic acid (HA) was achieved using 1-ethyl-(3-dimethylaminopropyl)-3-carbodiimide (EDC) and *N*-hydroxysuccinimide (NHS) in a mixed solvent of water and DMF (*v*/v, 1:1), yielding a brush polymer, namely HA-BK. HA-BK underwent deprotection reaction in the presence of trifluoroacetic acid (TFA), affording the target product, namely HA-K where K was short for poly($_L$-lysine). The successful synthesis of HA-K was confirmed by ^{1}H NMR spectroscopy (Fig. S1). The degree of substitution (DS) of HA was defined as the number of poly($_L$-lysine) per 100 $_D$-glucuronic acid of HA. It was determined by ^{1}H NMR based on the peak areas corresponding to the *n*-butyl end group of poly($_L$-lysine) protons and *N*-acetyl-$_D$-glucosamine and $_D$-glucuronic acid residues of HA protons. HA-K with DS values of 4.0, 7.2, 10.1, and 10.8 was synthesized to modulate the antibacterial properties.

As the pH increased, HA-K underwent deprotonation (Fig. 2A and Fig. S3), leading to a gradual decrease in Zeta potential. HA-K with a DS of 7.2–10.8 reached electrical neutrality within the pH range of 6–7. Under acidic conditions, its positive Zeta potential indicates that it predominantly presents cationic groups, which may confer bactericidal activity in the biofilm microenvironment. The Zeta potential of HA-K (DS = 4.0) was always below zero at pH 3.5–9.5, due to the increased ratio of carboxylic acid groups to amino groups in a single polymer. Dynamic light scattering (DLS) was used to investigate the self-assembly behavior of HA-K in aqueous solutions. At pH 7.4, HA-K (100 μg/mL) with DS of 4.0–10.8 showed hydrodynamic diameters (i.e., sizes) ranging from 300 to 400 nm (Fig. 2B and S4), suggesting the formation of PECs. The size of HA-K PEC under acidic conditions (pH 5.5) showed no significant difference as compared to that under physiological conditions (pH 7.4). The morphology was observed by transmission electron microscopy (TEM), which revealed spherical self-assemble structure of HA-K PEC in aqueous solution (Fig. 2C). The overall distribution was fairly uniform, and the diameters determined by TEM were consistent with the DLS results. NaCl, urea, and sodium dodecyl sulfate (SDS) were used to disrupt intermolecular electrostatic interactions, hydrogen

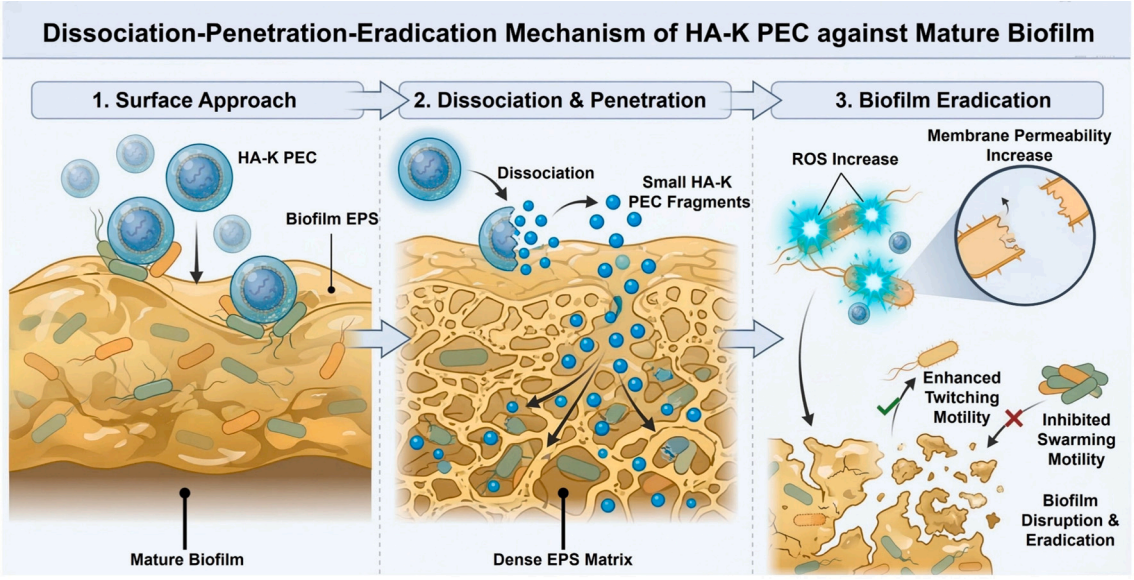

Fig. 1. Schematic illustration of biofilm penetration and eradication mechanisms of HA-K PEC. Nanobanana and Biorender were used to create this figure.

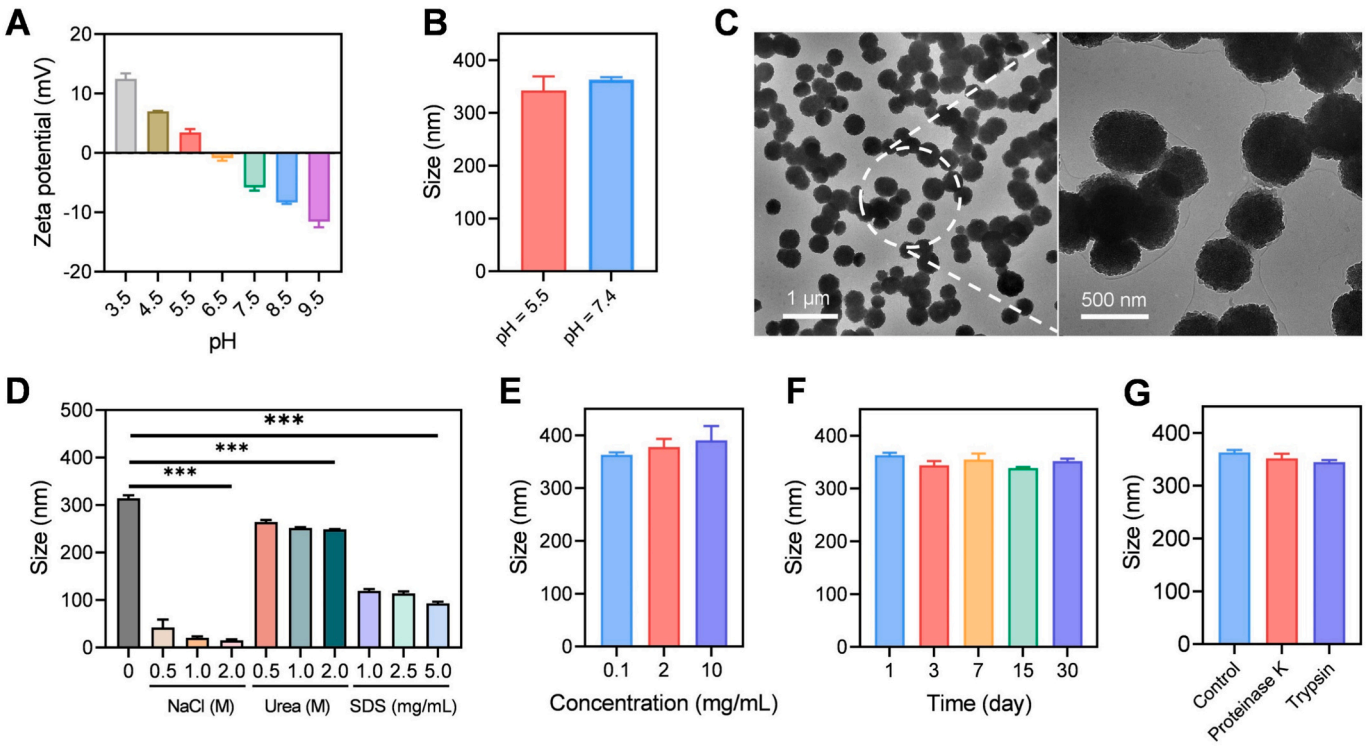

Fig. 2. (A) Zeta potentials of HA-K at pH 3.5–9.5. (B) Sizes of HA-K PEC at pH 5.5 and 7.4. (C) TEM images of HA-K PEC at different magnifications. (D) The effects of NaCl, urea, and SDS on the sizes of HA-K PEC. (E) Sizes of HA-K PEC at different concentrations. (F) Durability of HA-K PEC aqueous solutions. (G) Enzymatic degradation stability of HA-K PEC (0.1 mg/mL in PBS, 24 h, 37 °C). Data are mean ± standard deviation (SD) ($n = 3$) (***$p < 0.001$).

bonds, and hydrophobic interaction of HA-K PEC in aqueous solutions, respectively (Fig. 2D). HA-K PEC dissociated to a great extent with addition of NaCl (e.g., 0.5 M), indicating that intermolecular electrostatic interaction is the main attractive force driving the formation of HA-K PEC. Significant dissociation of HA-K PEC can be observed by addition of SDS (e.g., 1.0 mg/mL), indicating that hydrophobic interaction between adjacent HA-K chains also plays an important role in the formation of PEC. Intermolecular hydrogen bonding interactions also contributed to the formation of HA-K PEC as evidenced by the decrease in their sizes with the addition of urea. In addition, HA-K PEC showed good stability against concentration variations (0.1–10 mg/mL, Fig. 2E). No phase separation was observed even at 100 mg/mL in PBS (Fig. S5). It also showed good durability that size of HA-K PEC barely changed within 30 days (0.1 mg/mL, Fig. 2F). Proteases, such as proteinase K and trypsin were unable to degrade HA-K PEC within a short time (i.e., 0–48 h) (Fig. 2G and S6A), potentially avoiding the degradation by bacteria prior to antibacterial treatment. HA-K PEC also showed good serum stability by incubating with mouse serum at 37 °C for 0–48 h (Fig. S6B). The good stability of HA-K PEC makes it ready to be used in vivo.

2.2. Prevention of bacterial biofilm formation

HA inhibited 77.9% and 79.0% biofilm growth of *S. aureus* and *E. coli*, respectively (Fig. 3A). The cationic poly(L-lysine) (K_{10}) exhibited limited efficacy of biofilm inhibition (inhibited 46.2% *S. aureus* and 72.6% *E. coli* biofilm growth). In comparison, HA-K PEC inhibited ≥97.8% bacterial biofilm growth (Fig. 3A), outperforming the linear polymers (i.e., HA and K_{10}) and their blend (i.e., HA + K_{10}). These results highlight the importance of the brush-like architecture and covalent integration of HA and poly (L-lysine). The DS also affected the efficacy of biofilm inhibition of HA-K PEC. Specifically, HA-K PEC (DS = 7.2) exhibited the highest efficacy of biofilm inhibition (97.8%) against *S. aureus*, whereas HA-K PECs (DS = 4.0, 10.1 and 10.8) only inhibited ≤93.2% *S. aureus* biofilm growth (Fig. S7). A similar trend was observed in terms of preventing of *E. coli* biofilm formation. Overall, all HA-K PECs showed potent biofilm inhibition and eradication properties. DS ranging from 4.0 to 10.8 displayed an insignificant effect (< 5%) on the efficacy of biofilm inhibition and eradication of HA-K PEC. HA-K PEC (DS = 7.2) was used as the model compound because of its most potent antibiofilm properties. We reasoned that HA-K PEC with different DS should possess the same antibiofilm mechanisms as HA-K PEC (DS = 7.2).

The minimum biofilm inhibitory concentration (MBIC) of HA-K PEC (DS = 7.2) was 37.5 μg/mL for both *S. aureus* and *E. coli* (Fig. 3B). It was much lower than the minimum inhibitory concentration (MIC, Fig. S8) and the minimum bactericidal concentration (MBC, Fig. S9). The MIC and MBC of HA-K PEC (DS = 7.2) for *S. aureus* and *E. coli* were ≥ 400 μg/mL. Bacterial cell viability treated with HA-K PEC (DS = 7.2) was further measured by flow cytometry using a SYTO 9/PI staining assay (Fig. S10). HA-K PEC (DS = 7.2) showed insignificant bactericidal effect on both *S. aureus* and *E. coli*. This suggested that inhibition of biofilm growth using HA-K PEC is independent of the bactericidal mechanism, thereby reducing the likelihood of bacteria developing resistance to the material. To verify this point, we conducted a bacterial drug resistance assay (Fig. S11). In the antibiotic group, the MBICs of vancomycin and tobramycin against *S. aureus* and *E. coli* increased to 128-fold and 64-fold, respectively, as compared to the initial values. In contrast, the MBIC of HA-K PEC remained unchanged, indicating that HA-K PEC did not induce the emergence of bacterial drug resistance. Quantitative reverse transcription polymerase chain reaction (qRT-PCR) was used to investigate the key genes (mprF and clfB) of *S. aureus* after HA-K PEC or antibiotics (e.g., vancomycin) treatments. mprF gene involved in pathways related to antimicrobial peptide/cationic antimicrobial substance tolerance. The vancomycin treated *S. aureus* increased the expression of mprF gene (Fig. S12), indicating the raise of drug resistance. In comparison, the HA-K PEC treated *S. aureus* maintained the mprF gene expression level further verified the inhibition of drug resistance. In addition, the clfB gene expression level was suppressed by HA-K PEC,

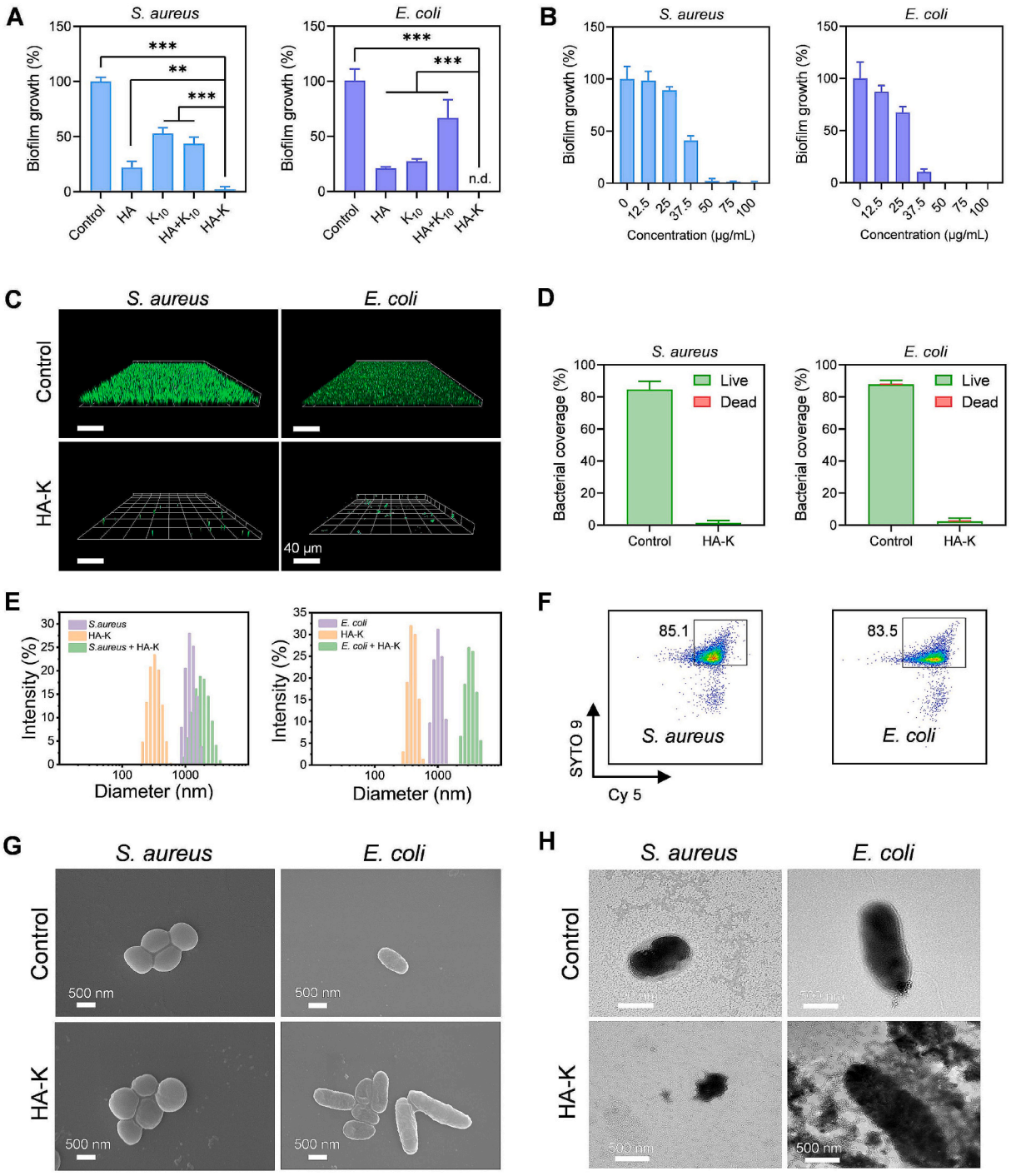

Fig. 3. The efficacy and mechanism of biofilm inhibition using HA-K PEC (DS = 7.2). (A) Biofilm growth of *S. aureus* and *E. coli* inhibited by PBS (the control), HA, K_{10}, HA + K_{10}, and HA-K PEC (50 μg/mL in PBS). (B) Biofilm growth of *S. aureus* and *E. coli* inhibited by HA-K PEC at different concentrations. (C) CLSM images of *S. aureus* and *E. coli* biofilm growth untreated or treated by HA-K PEC. (D) Coverage of *S. aureus* and *E. coli* untreated or treated by HA-K PEC. (E) HA-K PEC induced bacterial aggregation determined by DLS. (F) Flow cytometry assay of the binding efficiency between bacteria and HA-K PEC. (G) SEM and (H) TEM images of planktonic bacteria untreated (control) and treated with HA-K PEC (Scale bar = 500 nm). Data are mean ± SD ($n = 3$) (**$p < 0.01$, ***$p < 0.001$). n.d. signifies not detected.

suggesting the inhibition of *S. aureus* adhesion.

We then employed confocal laser scanning microscopy (CLSM) to provide a more intuitive assessment of biofilm inhibition by HA-K PEC. As shown in Fig. 3C and D, both *S. aureus* and *E. coli* biofilm formation were effectively inhibited in the presence of HA-K PEC, with only sporadic bacterial colonization observed on the surface of the vessel and minimal dead bacteria detected.

2.3. Biofilm inhibition mechanism of HA-K PEC

The interactions between HA-K PEC and bacteria were initially investigated by DLS (Fig. 3E). Bacteria aggregation was observed for both *S. aureus* and *E. coli* after mixing with HA-K PEC as evidenced by the significant increase in their sizes. In addition, bacteria aggregation induced by HA-K PEC was further observed under CLSM (Fig. S13). These phenomena indicated that HA-K PEC can bind with multiple

bacteria, leading to bacterial aggregation.

Staphylococcal protein A (SPA) is a surface protein of *S. aureus* and plays a vital role in maintaining bacterial structural integrity [31]. Moreover, SPA would bind to immunoglobulin G (IgG), promoting bacterial adhesion and subsequent infection [32]. Therefore, antibacterial materials that can efficiently bind to SPA provide a promising strategy to inhibit *S. aureus* biofilm formation. Consequently, we focused on the interaction between HA-K PEC and SPA. We measured the circular dichroism (CD) spectra of HA-K PEC, SPA and their mixture. Poly ($_L$-lysine) side-chains of HA-K adopted a random coil conformation due to the short peptide chain length while SPA predominantly adopted an α-helical conformation in PBS (Fig. S14). For the SPA and HA-K PEC mixture, the helicity of SPA significantly decreased suggesting that HA-K PEC can bind to SPA and break the intramolecular hydrogen bonds of a helix domain. We quantitatively assessed the binding affinity between HA-K PEC and SPA (Fig. S15-S16). The binding constants of HA-K PEC to SPA are all above 10^5 M^{-1} (Table S2), outperforming both HA (K_b = 9.65 × 10^4 M^{-1}) and K_{10} (K_b = 4.19 × 10^3 M^{-1}). It is interesting to observe that HA-K PEC (DS = 7.2) and SPA has the K_b of 1.3 × 10^6 M^{-1} which is close to the K_b of weak antibody-antigen.

Flow cytometry was used to determine the binding efficiency of HA-K PEC toward bacteria (Fig. 3F). It is interesting to observe that HA-K PEC (DS = 7.2) exhibited high binding efficiency (Fig. S17) toward *S. aureus* (85.1%) and *E. coli* (83.5%). This phenomenon likely arises from multivalent interactions between HA-K PEC and bacteria, including electrostatic, hydrophobic, and hydrogen-bonding interactions. We presume that HA-K PEC should also have potentially high binding efficiency toward commensal bacteria because of the multivalent interactions between HA-K PEC and bacteria. We also reason that HA-K PEC should be non-lethal to the beneficial microbiota, providing a way to replace broad-spectrum antibiotics that are lethal to the beneficial microbiota.

The surfaces of untreated planktonic bacteria were smooth, whereas HA-K PEC–treated planktonic bacteria exhibited surface wrinkling, as shown by both SEM (Fig. 3G) and TEM (Fig. 3H). Nevertheless, the membranes of HA-K PEC–treated planktonic bacteria remained intact and undamaged, as further confirmed by the membrane permeability assay. In this experiment, the PI fluorescence intensity of bacteria did not significantly increase after exposure to HA-K PEC, indicating that HA-K PEC did not alter bacterial membrane permeability (Fig. S18). It is worth noting that the assembled structure of HA-K PEC was not observed by TEM (Fig. 3H). Bacteria on surfaces were also observed under SEM (Fig. S19). Planktonic bacteria can readily grow biofilms on the surfaces without any treatment. In comparison, bacterial biofilms were significantly inhibited by HA-K PEC as evidenced by the observation of only sporadic bacterial adhesion.

2.4. Biofilm eradication and penetration properties of HA-K PEC

We further investigated the biofilm eradication property of HA-K PEC. Specifically, 1-day-old biofilm was incubated with HA-K PEC for 24 h. HA-K PEC eradicated ≥84.3% and 85.6% 1-day-old *S. aureus* and *E. coli* biofilm biomass at 50 μg/mL (Fig. 4A), outperforming linear polymers (i.e., HA and K_{10}), blend of linear polymers (i.e., HA + K_{10}) and common antibiotics (Fig. S20).

HA-K PEC with a moderate substitution degree (DS = 7.2) showed the highest biofilm eradication efficacy, achieving eradication rate 91.0% for *S. aureus* and 89.5% for *E. coli*. HA-K PECs (DS = 4.0, 10.1 and 10.8) eradicated ≤88.3% *S. aureus* biofilm and ≤ 88.2% *E. coli* biofilm (Fig. S21). Moreover, we determined the minimum biofilm eradication concentration (MBEC) of HA-K PEC for both bacterial strains, finding that the MBECs for *S. aureus* and *E. coli* were 75 μg/mL and 50 μg/mL, respectively (Fig. 4B). HA-K PEC (DS = 7.2) also exhibited biofilm eradication property against more mature biofilms (i.e., 3-day-old and 5-day-old, Fig. 4C-4D). It showed higher biofilm eradication rates against *E. coli* biofilms than those of *S. aureus* biofilms with 3 or 5 day maturities, indicating strain-dependent difference. This phenomenon presumably originated from the distinct EPS structures of *E. coli* and *S. aureus* biofilms. HA-K PEC should have higher permeation efficiency in mature *E. coli* biofilms.

CLSM was further used to investigate the biofilm eradication property of HA-K PEC (Fig. 4E and Fig. 4F). HA-K PEC (DS = 7.2) eradicated ≥99% of 1-day-old biofilms formed by both *S. aureus* and *E. coli*. The biofilm penetration property of HA-K PEC was also investigated by CLSM. Specifically, *S. aureus* and *E. coli* were cultured on PDMS surfaces for 1 day (d), 3 d, and 5 d, respectively, followed by staining with SYTO 9. Rhodamine B-labeled HA-K PEC PBS solution (DS = 7.2, 50 μg/mL) was added to the biofilm surface. It was removed at predetermined times, and the resulting biofilm was observed under CLSM.

HA-K PEC can efficiently penetrate in both 1-day-old and 3-day-old biofilms within 2 h (Fig. S22) as evidence that the yellow fluorescence filled the entire biofilm. It also demonstrated potent biofilm penetration property toward 5-day-old biofilms of both *S. aureus* and *E. coli* (Fig. 4G). We have performed a layer-by-layer tomographic scanning along the vertical *Z*-axis of the biofilm to spatially quantify the penetration property of HA-K PEC (Fig. S23-S24). For all *S. aureus* and *E. coli* biofilms with different maturities, HA-K PEC was able to penetrate dense EPS barriers and effectively enrich to the deep layers of biofilms as evidence that the red fluorescence peak (exclusively from Rhodamine B-labeled HA-K PEC) shifts toward lower numbered layers and maintains a high signal throughout the entire layer. As the maturity of the biofilm increases, the biofilm penetration efficiency gradually decreases. Nonetheless, HA-K PEC can still efficiently penetrate 5-day-old biofilms within 8 h. In addition, it demonstrated higher permeation efficiency in *E. coli* biofilms.

2.5. Biofilm eradication mechanism of HA-K

Generally, the pore size of biofilm EPS is approximately 200 nm, which is smaller than the size of HA-K PEC (300–400 nm). From this perspective, HA-K PEC would not be expected to penetrate biofilms unless it can disrupt the EPS or dissociate into smaller self-assembled structures. A common approach to evaluate whether materials disrupt and reduce biofilm EPS is to measure changes in extracellular protein and polysaccharide contents. The results showed that, regardless of biofilm maturity, HA-K PEC significantly decreased protein and exopolysaccharide levels in both types of bacterial biofilms (Fig. 5A and B), indicating that HA-K PEC can effectively reduce the EPS content of biofilms. EPS protein and eDNA staining assays were used to further verify EPS disruption following HA-K PEC treatment (Fig. S25-S26). For both *S. aureus* and *E. coli* biofilms, HA-K PEC was able to decrease EPS protein and eDNA contents from outer to inner layers of the biofilms.

Furthermore, we extracted water-soluble EPS from the *S. aureus* biofilm using the methanol-phenol method. The particle size of the extracted EPS was about 430 nm, whereas the blend composed of HA-K PEC and EPS was around 70 nm, indicating dissociation of both EPS and HA-K PEC (Fig. 5C). This result supports our proposed mechanism that HA-K PEC disrupts the EPS structure and dissociates, thereby facilitating biofilm penetration.

The dissociation of HA-K PEC induced by extracted EPS was further verified by fluorescence spectroscopy. An aggregation-induced emission (AIE) dye [33], namely 4-(1,2,2-triphenylvinyl)phenyl (TPE) was covalently incorporated into HA-K. TPE-labeled HA-K PEC exhibited a strong fluorescence peak at 500 nm due to its aggregation (Fig. 5D). After interaction with EPS, the fluorescence intensity at 500 nm significantly decreased, indicating dissociation of the HA-K PEC.

Besides biofilm EPS, HA-K PEC also interacted with biofilm bacteria. Unlike planktonic bacteria, HA-K PEC significantly increased the membrane permeability of biofilm bacteria (Fig. 5E). We assumed that the acidic microenvironment of biofilms (e.g., pH 5.5) [34,35] caused HA-K PEC to maintain an overall positively charged surface and enhanced its interaction with the negatively charged bacteria, resulting

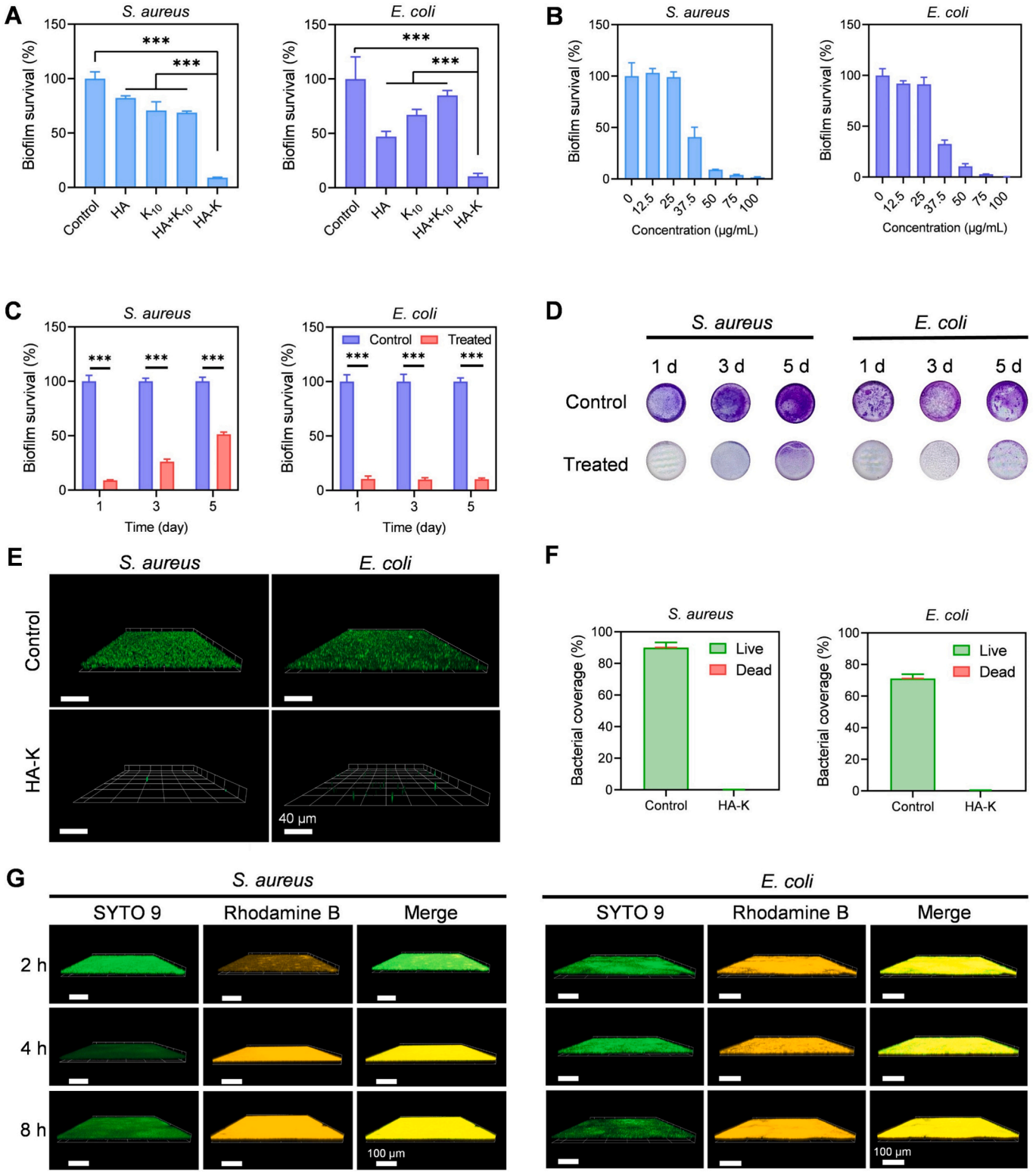

Fig. 4. Biofilm eradication and penetration properties of HA-K PEC. (A) Biofilm survival of *S. aureus* and *E. coli* eradicated by PBS (the control), HA, K_{10}, HA + K_{10}, and HA-K PEC (50 μg/mL in PBS). (B) Biofilm survival of *S. aureus* and *E. coli* eradicated by HA-K PEC at different concentrations. (C) Biofilm survival of *S. aureus* and *E. coli* biofilms (1-day-old to 5-day-old) eradicated by HA-K PEC (50 μg/mL in PBS). (D) Representative images of crystal violet stained *S. aureus* and *E. coli* biofilms (1-day-old to 5-day-old) eradicated by HA-K PEC (50 μg/mL in PBS). (E) CLSM images of *S. aureus* and *E. coli* biofilms (1-day-old) untreated (control) or treated by HA-K PEC. (F) Coverage of *S. aureus* and *E. coli* biofilms (1-day-old) untreated (control) or treated by HA-K PEC. (G) Penetration of HA-K PEC in *S. aureus* and *E. coli* biofilms (5-day-old) at 2 h, 4 h, and 8 h intervals (scale bar = 100 μm). The biofilms were stained with SYTO 9. Rhodamine-B-labeled HA-K PEC was used for biofilm penetration. Data are mean ± SD ($n = 3$) (***$p < 0.001$).

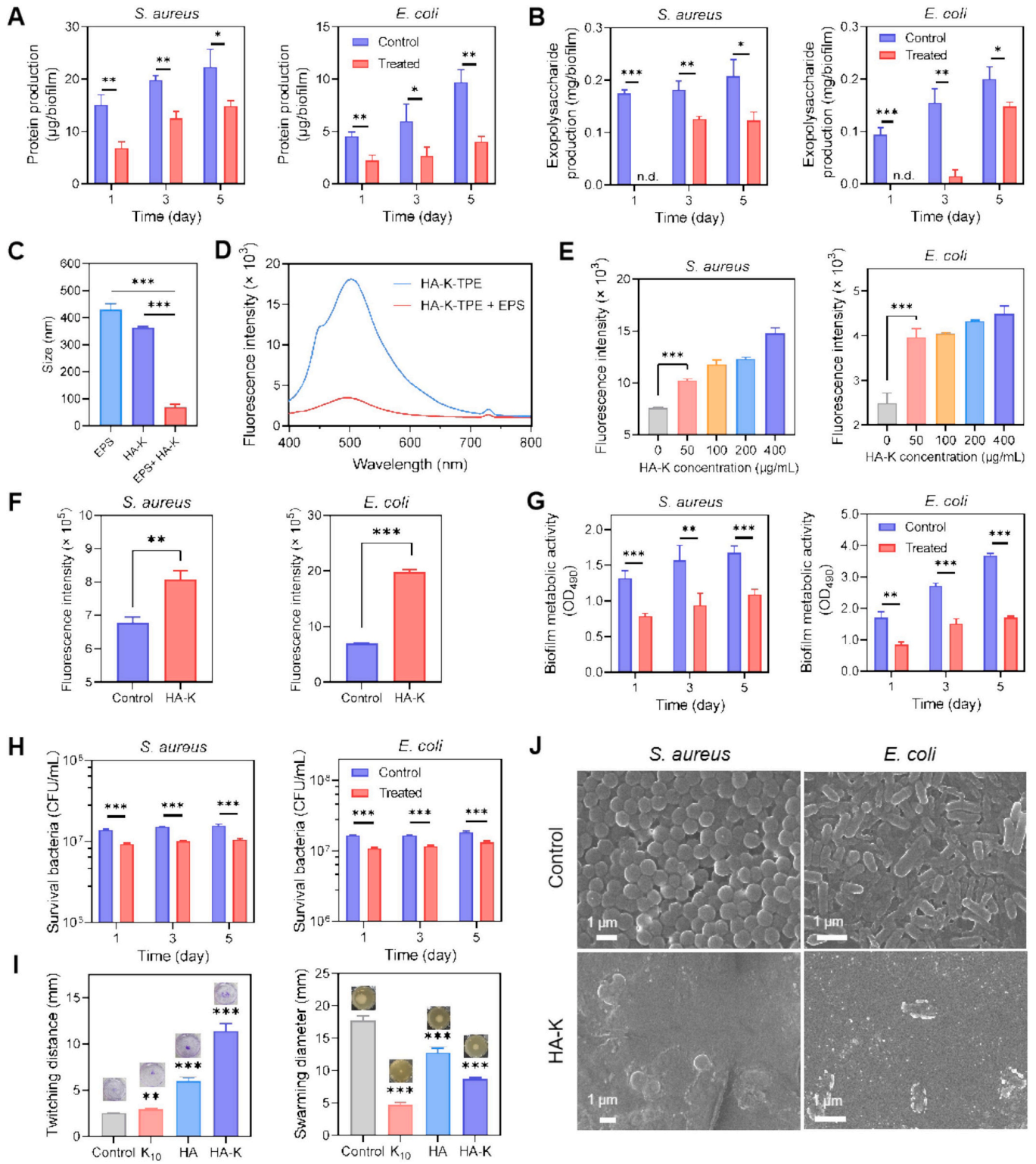

Fig. 5. Exploration of the biofilm eradication mechanism of HA-K PEC (DS = 7.2). (A) The effect of HA-K PEC on the protein content of biofilms. (B) The effect of HA-K PEC on the extracellular polysaccharide content of biofilms. (C) Sizes of extracted EPS, HA-K PEC, and their blend. (D) Fluorescence spectra of TPE-labeled HA-K PEC before and after interaction with the extracted EPS. (E) The effect of HA-K PEC concentration on membrane permeability of biofilm bacteria. (F) The effect of HA-K PEC on the ROS production of biofilms. (G) Metabolic activity of biofilms treated with HA-K PEC. (H) Survival of biofilm bacteria treated with HA-K PEC. (I) Assessment of twitching and swarming motilities of *E. coli* treated with K_{10}, HA, and HA-K PEC. (J) SEM images of biofilm bacteria before and after treatment with HA-K PEC (Scale bar = 1 μm). All samples were tested at 50 μg/mL in PBS. Data are mean ± SD ($n = 3$). (*$p < 0.05$, **$p < 0.01$, ***$p < 0.001$). n.d. signifies not detected.

in increased membrane permeability.

Additionally, HA-K PEC elevated the production of ROS in the biofilm (Fig. 5F). We have verified that HA-K PEC itself was not able to generate any ROS. ROS are frequently generated by bacterial aerobic respiration. It is reported that carbonyl cyanide *m*-chlorophenylhydrazone (CCCP) could interfere with respiratory processes of bacteria by inhibition of ATP synthesis [36]. The production of ROS in HA-K PEC treated bacterial biofilms was significantly suppressed in the presence of CCCP (Fig. S27), indicating a secondary bacterial stress response induced by HA-K PEC interactions.

The increase of bacterial membrane permeability and ROS production in biofilms should lead to bacterial cell death after HA-K PEC treatment. Indeed, the biological activity and survival of bacteria in the biofilms were significantly reduced after HA-K PEC treatment (Fig. 5G, H and S28). Cell viability of bacteria within biofilms was further measured by flow cytometry using a SYTO 9/PI staining assay (Fig. S29). HA-K PEC (DS = 7.2) showed significant bactericidal effect on both *S. aureus* and *E. coli* in respective biofilms ascribing to contact killing from electrostatic interactions and ROS stress-induced killing.

Bacterial twitching and swarming are key modes of motility. Twitching motility, driven by surface fimbriae, is typically observed in certain Gram-negative bacteria, such as *E. coli* and *P. aeruginosa* [37,38]. When bacteria attach to surfaces, they migrate toward the attachment site to seek essential nutrients through mechanisms such as swarming motility [39–41]. Therefore, twitching and swarming motility play vital roles in biofilm formation and dissociation. Consequently, we investigated the effect of HA-K PEC on the twitching and swarming of *E. coli* motilities (Fig. 5I). HA-K PEC significantly enhanced bacterial twitching motility, such that the diameter of bacterial movement was five times greater than that of the control group. This increased motility hindered the ability of bacteria to rapidly adhere to surfaces during the initial colonization phase. Therefore, HA-K PEC significantly enhanced bacterial twitching motility, outperforming K_{10} and HA in terms of hindering biofilm formation and promoting the dispersion and dissociation of pre-existing biofilms. HA-K PEC can inhibit bacterial swarming motility, thereby significantly reducing bacterial aggregation. This inhibition contributed substantially to the inhibition and eradication of biofilms. K_{10} exhibited the most pronounced inhibition efficacy on bacterial swarming motility while HA-K PEC demonstrated better inhibition efficacy than HA, indicating that the inhibition mechanism of swarming motility was primarily related to the poly(L-lysine) chains.

SEM was used to observe the morphologies of biofilm bacteria treated with HA-K PEC (Fig. 5J). It revealed that HA-K PEC effectively eradicated the majority of *S. aureus* and *E. coli* in respective biofilms. Additionally, HA-K PEC re-assembled on the surfaces of biofilm bacteria, leading to the rupture and death of bacteria.

2.6. *In vivo* prevention and treatment of biofilm associated infections and assessment of biosafety of HA-K PEC

We further evaluated the in vivo biofilm inhibition and eradication properties of HA-K PEC (DS = 7.2). In the biofilm inhibition mouse model, we created artificial wounds on the subcutaneous area of the mouse back, inserted PDMS slides into the wounds, and sutured them. We then injected *S. aureus* suspensions along with HA-K PEC solutions to the wounds. The slides were retrieved on day 3 and day 7 post-administration, followed by quantification of the bacterial content on the slides (Fig. 6A). In the biofilm eradication mouse model, we inserted the 1-day-old *S. aureus* biofilm coated PDMS slides into the subcutaneous area of the mouse back, followed by surgical suturing. Then, HA-K PEC solutions were injected into the wounds (Fig. 6B).

As illustrated in Fig. 6C, HA-K PEC significantly inhibited biofilm formation on the implanted slides (inhibited ≥95.2% and 99.7% of bacterial biofilm growth) in vivo on day 3 and day 7 post-administration. SEM was used to investigate the potential biofilm growth on the implanted slides (Fig. S30). The untreated implant surface was completely covered by the biofilm containing a large number of *S. aureus* cells. In comparison, the HA-K PEC treated implant surface was adhered by few *S. aureus* cells without any biofilm growth. Hematoxylin and eosin (H&E) staining assay was used to analysis the histopathology of planktonic *S. aureus* infected PDMS slide surrounding tissues (Fig. S31). After 3 and 7 days of implantation, untreated (control) mouse skin tissues were full of inflammatory cells, whereas HA-K PEC treated mouse skin tissues showed significantly inhibited inflammatory reaction.

HA-K PEC also exhibited high biofilm eradication property (eradicated ≥64.6% and 63.9% of bacterial biofilm) in vivo on day 3 and day 7 post-administration (Fig. 6D). SEM was used to observe biofilm morphologies on the implanted slides after HA-K PEC treatment (Fig. S32). The *S. aureus* biofilm on implant surface was efficiently disrupted by HA-K PEC as compared to the untreated surface. The biofilm eradication of HA-K PEC should involve the efficient biofilm penetration via dissociation into smaller nanoparticles, disruption of the EPS matrix via multiple interactions, regulation bacterial twitching/swarming motility, increasing ROS production and bacterial cell membrane permeability. In terms of the EPS disruption mechanisms, HA-K PEC possesses a chemical way to interact and dissociate the biofilm EPS which is distinct from previous reported physical EPS disruption mechanism (e.g., ultrasonic cavitation) [42,43]. While the physical EPS disruption showed a much shorter treatment time (e.g., 5–10 min), it required additional facilities, such as ultrasonic therapeutic apparatus. Histopathological analysis revealed severe inflammatory response that large number of inflammatory cells accumulated in the tissues around the *S. aureus* biofilm infected PDMS slides after 3 and 7 days of implantation (Fig. S33). After HA-K PEC treatment, the tissues around the *S. aureus* biofilm infected PDMS slides showed significantly alleviated inflammation reaction after 3 and 7 days of implantation, suggesting potent in vivo biofilm eradication properties.

Additionally, we collected blood samples to measure the levels of inflammatory factors and found that HA-K PEC could reduce the content of TNF-α in the body, thereby alleviating bacterial-induced infections (Fig. 6C-6D). Fluorescence imaging was employed to investigate the absorption and distribution of HA-K PEC in vivo. Specifically, Cy5-labeled HA-K PEC (50 μg/mL in PBS) was subcutaneously injected into the dorsal region of normal mice. The fluorescence distribution in major organs (heart, liver, spleen, lung, and kidney) was evaluated at predetermined intervals using a 3D quantitative fluorescence imaging system (Fig. 6E). HA-K PEC mainly distributed in the liver and kidney. Fluorescence intensity in these organs gradually increased within 4 h, followed by a steady decrease, and complete disappearance by 48 h post-administration. This suggests that HA-K PEC is primarily metabolized and excreted through the liver and kidney, respectively.

HA-K PEC exhibited negligible cytotoxicity toward NIH 3 T3 cells at ≤500 μg/mL (Fig. S34), which is much higher than its MBIC and MBEC. We also assessed the hemolytic properties of HA-K PEC. It also demonstrated low hemolysis (< 4%) even at 2000 μg/mL (Fig. S35). In addition, a mouse model was used to evaluate blood routine and blood biochemical indices of HA-K PEC (Fig. S36–S37). Statistical significance was not observed for HA-K PEC treated and untreated mice, indicating good blood compatibility.

2.7. Proteomic assessment of HA-K PEC treated *S. aureus*

To investigate the effect of HA-K on the protein expression of *S. aureus*, TMT-based quantitative proteomics analysis was conducted on both untreated and HA-K PEC treated planktonic *S. aureus*. A total of 2335 proteins were identified (unique peptides ≥1, FDR ≤ 0.01). Differentially expressed proteins (DEPs) were screened using the criteria of fold change (FC) > 2 (or < 0.5) and *p*-value <0.01. As shown in Fig. 7A, 756 DEPs were identified, with 594 up-regulated and 162 down-regulated. Next, the cell components in the Gene Ontology (GO) database were annotated and counted. The subcellular localization of DEPs

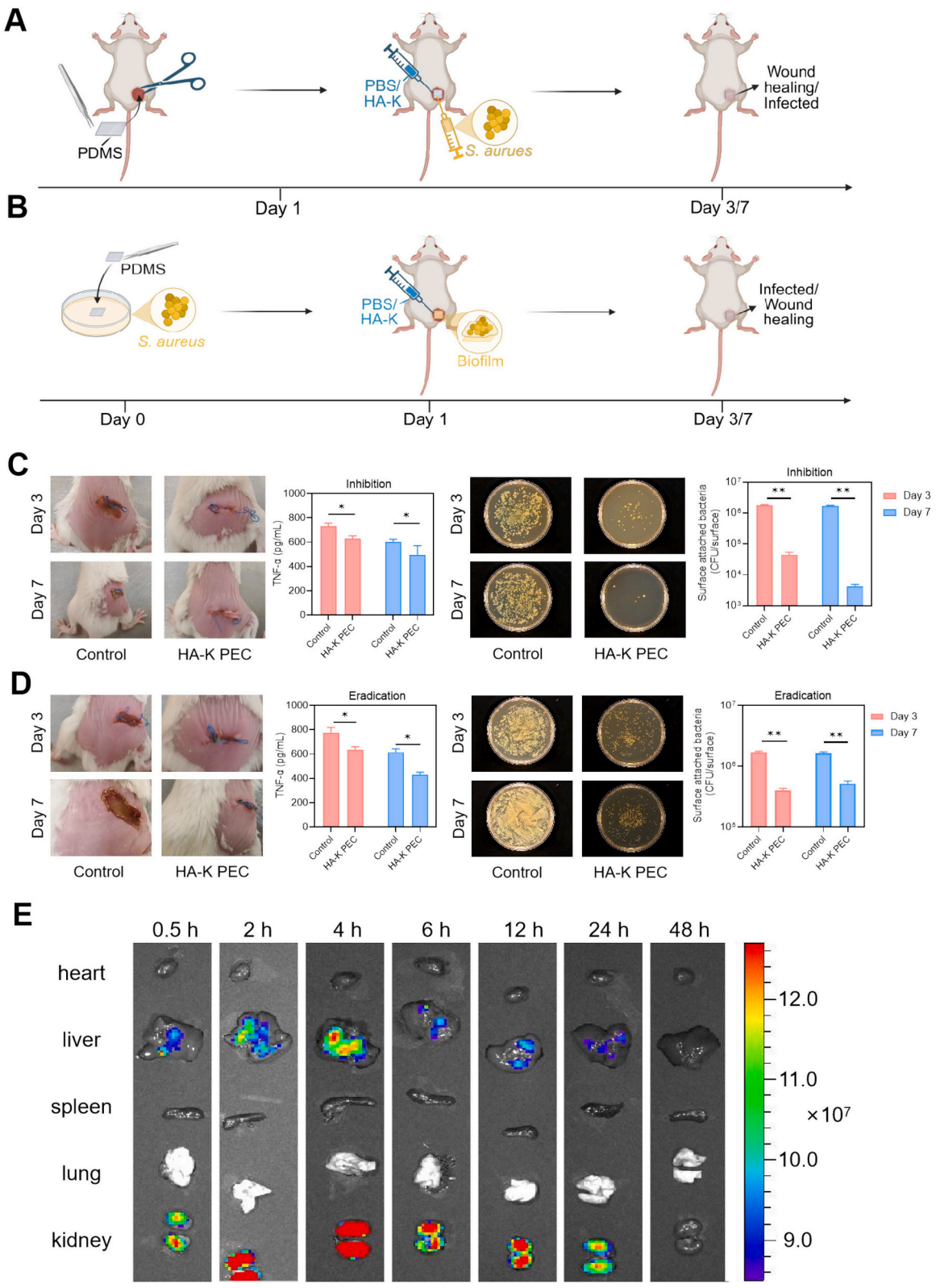

Fig. 6. (A) Schematic diagram of prevention of biofilm-associated infection using a subcutaneous implantation mouse model in the back. (B) Schematic diagram of treatment of biofilm-associated infection using the subcutaneous implantation mouse model in the back. (C) Representative images of the mouse's backs and the LB agar plates untreated (control) and treated with HA-K PEC to prevent biofilm growth on the implants after administration. The level of TNF-α in vivo untreated (control) and treated with HA-K PEC on day 3 and day 7 post-administration. (D) Representative images of the mouse's backs and the LB agar plates untreated and treated with HA-K PEC to eradicate biofilms on the implants after administration. The level of TNF-α in vivo untreated (control) and treated with HA-K PEC on day 3 and day 7 post-administration. (E) Fluorescence imaging was performed in the heart, liver, spleen, lung and kidney at specified time points following the injection of Cy5-labeled HA-K PEC. Data are mean ± SD ($n = 3$). (*$p < 0.05$, **$p < 0.01$).

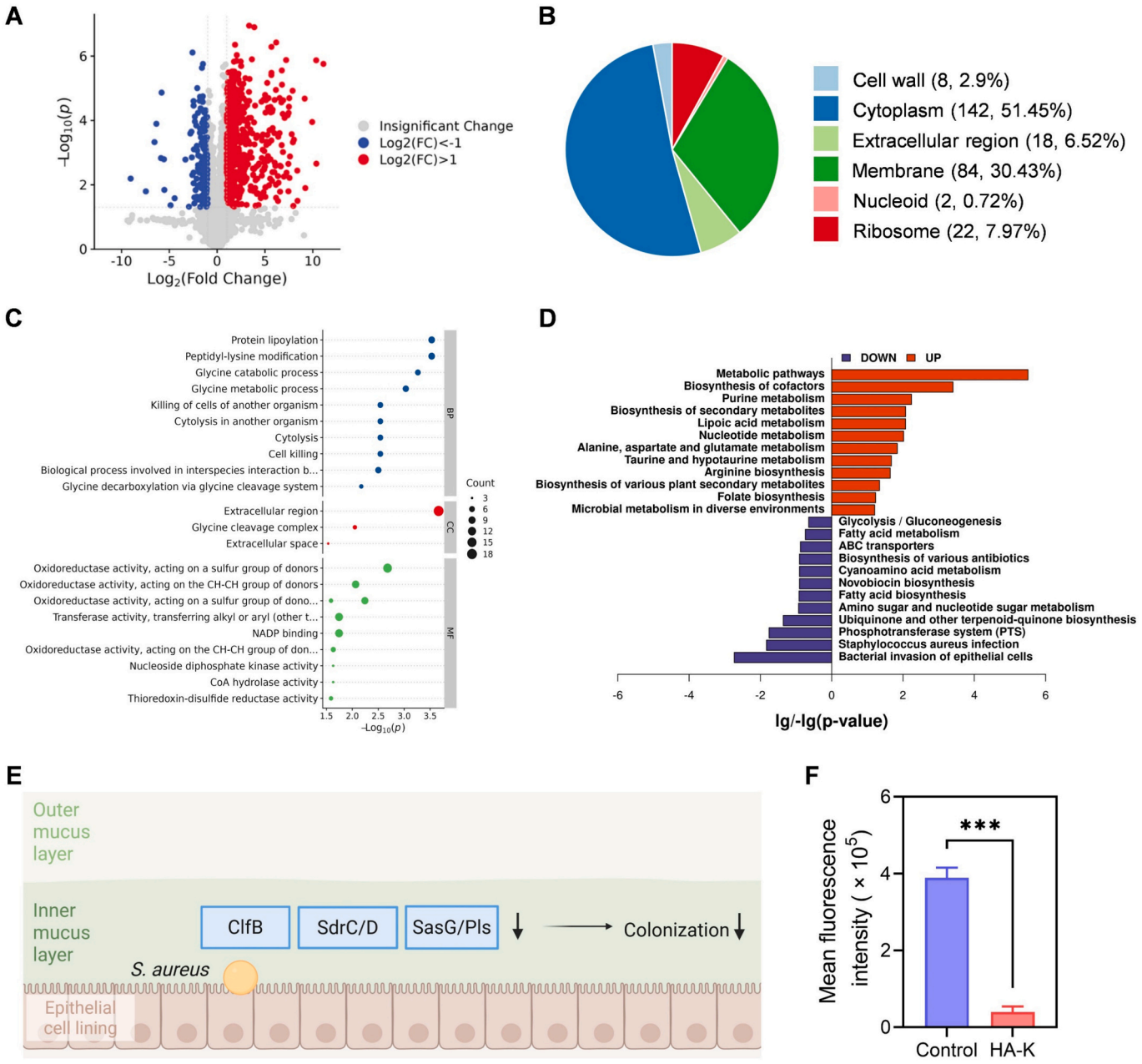

Fig. 7. Proteomic analysis of *S. aureus* treated with HA-K PEC. (A) Volcano plot of DEPs, (B) subcellular localization of DEPs, (C) GO enrichment analysis of DEPs, and (D) butterfly diagram of KEGG pathway enrichment of up-regulated and down regulated proteins between the control group and the HA-K PEC-treated group. (E) Schematic diagram HA-K PEC-treated group partial protein levels of *S. aureus* infection pathways. (F) Fluorescence intensity of epithelial cells after incubation with bacteria exposed to Cy5-labeled HA-K PEC. Data are mean ± SD ($n = 3$). (***$p < 0.001$).

enriched into the cell components category in the GO database revealed that 51.45% were located in the cytoplasm, 30.43% in the cell membrane, 7.97% in the ribosome, 6.52% in the extracellular region, 2.90% in the cell wall and 0.72% in the nucleoid (Fig. 7B), indicating that HA-K PEC predominantly affects the cytoplasm and cell membrane of *S. aureus*. The clustering heatmap (Fig. S38) illustrates significant changes in the protein expression patterns of HA-K PEC treated *S. aureus*, with columns representing different samples and rows representing individual proteins. Red indicates highly expressed proteins, while blue indicates low-expression proteins.

DEPs were classified into three GO categories: biological processes, molecular function, and cellular components, with the top 20 GO terms shown in Fig. 7C. The molecular functions associated with DEPs included catalytic activity, binding, transporter activity, and transcriptional regulatory activity. In biological processes, DEPs were involved in cellular processes, metabolic processes, biological regulation, and localization. Kyoto Encyclopedia of Genes and Genomes (KEGG) pathway analysis identified a total of 99 pathways associated with DEPs, categorized into five groups: metabolism, genetic information processing, environmental information processing, cellular processes, and human diseases (Fig. 7D). Notably, the majority of DEPs were associated with the metabolism pathway, with 79 DEPs annotated as involved in metabolic processes. This suggests that the metabolic activity of *S. aureus* treated with HA-K PEC significantly increased, implying that bacterial activity was enhanced rather than inhibited, which aligns with the previous experimental findings that HA-K PEC did not inhibit bacterial activity at a concentration of 100 μg/mL. Biofilm bacteria exhibited distinct proteomic and metabolic profiles as

compared to planktonic ones [44]. HA-K PEC also displayed different interactions with them. Specifically, HA-K PEC was non-lethal to planktonic bacteria with no influence on bacterial cell membrane permeability. In comparison, HA-K PEC became lethal to biofilm bacteria because of the acidic microenvironment. Fatty acids are essential components of cell membranes, and the inhibition of fatty acid synthesis can disrupt the formation of bacterial cell membranes and biofilms [45,46]. Based on the TMT-based quantitative proteomic analysis, HA-K PEC inhibited bacterial biofilm formation by reducing the metabolism and synthesis of fatty acids of *S. aureus*. qRT-PCR was used to investigate the fabD gene involved in fatty acids synthesis pathway. HA-K PEC-treated *S. aureus* exhibited reduced fabD gene expression (Fig. S39), indicating the reduction of fatty acid synthesis.

Additionally, *S. aureus* and epithelial cell binding was inhibited by HA-K PEC. Specific analysis of this pathway revealed that HA-K PEC downregulated the expression of clfB, SdrC/D, and SasG/Pls in *S. aureus*, thereby diminishing bacterial colonization of epithelial cells (Fig. 7E). The downregulation of clfB gene expression level of *S. aureus* treated by HA-K PEC further verified the inhibition of *S. aureus* adhesion and bacterium-host-cell-interactions as revealed by qRT-PCR (Fig. S39). To further verify the above discovery, we used flow cytometry to measure the binding between bacteria and epithelial cells. The results showed that the binding efficiency of *S. aureus* to epithelial cells was greatly reduced by HA-K PEC (Fig. 7F), suggesting that HA-K PEC can be readily used to prevent *S. aureus* binding and subsequent biofilm formation on epithelial cells and epithelial tissues.

3. Conclusion

We have demonstrated that the brush polyelectrolyte complex HA-K PEC effectively prevents and eradicates implant-associated biofilms, thereby addressing biofilm-related infections at both early and established stages. HA-K self-assembles into stable PECs that exhibit strong binding to planktonic bacteria and efficient penetration into mature biofilms. Mechanistically, HA-K PEC engages in multivalent electrostatic, hydrophobic, and hydrogen-bonding interactions, resulting in high affinity for planktonic bacteria, while its dissociation into smaller nanoparticles within the biofilm enables disruption of the EPS matrix and promotes biofilm clearance. Importantly, HA-K PEC displays negligible cytotoxicity toward mammalian cells and does not induce bacterial drug resistance. Collectively, these features position HA-K PEC as a promising non-antibiotic therapeutic platform for the simultaneous prevention and treatment of biofilm-associated infections on medical implants.

CRediT authorship contribution statement

Yu Liu: Writing – review & editing, Writing – original draft, Validation, Software, Methodology, Investigation, Formal analysis, Data curation. **Jin Shi:** Writing – review & editing, Writing – original draft, Validation, Methodology, Investigation, Formal analysis, Data curation. **Peng Wang:** Writing – review & editing, Investigation. **Zhiyong Liu:** Writing – review & editing, Investigation. **Tingting Cao:** Writing – review & editing, Investigation. **Dengwei Yu:** Writing – review & editing, Investigation. **Jingrui Shen:** Writing – review & editing, Investigation. **Lichen Yin:** Writing – review & editing, Supervision, Resources, Project administration, Funding acquisition. **Jianjun Cheng:** Writing – review & editing, Writing – original draft, Validation, Supervision, Resources, Project administration, Funding acquisition. **Haoyu Tang:** Writing – review & editing, Writing – original draft, Validation, Supervision, Software, Resources, Project administration, Methodology, Investigation, Funding acquisition, Conceptualization.

Declaration of competing interest

The authors declare that they have no known competing financial interests or personal relationships that could have appeared to influence the work reported in this paper.

Acknowledgements

This work was supported by “Pioneer” and “Leading Goose” R&D Program of Zhejiang (2024SDXHDX0004 for J.C.), the National Natural Science Foundation of China (52233015 for J.C.). J.C. acknowledges the support of the New Cornerstone Investigator Program, New Cornerstone Science Foundation. This work was also supported by Science and Technology Program of Suzhou (SKY2022111 for H.T.), H.T. acknowledges the support of Collaborative Innovation Center of Suzhou Nano Science & Technology, and FUNSOM Self-Directed Research Project (2022). Yu Liu thanks Biorender.com for the assistance of drawing of Fig. 6A, Fig. 6B and Fig. 7E.

Appendix A. Supplementary data

Supplementary data to this article can be found online at https://doi.org/10.1016/j.cej.2026.179623.

Data availability

Data will be made available on request.

References

[1] S. Barman, L.B. Kurnaz, R. Leighton, M.W. Hossain, A.W. Decho, C. Tang, Intrinsic antimicrobial resistance: molecular biomaterials to combat microbial biofilms and bacterial persisters, Biomaterials 311 (2024) 122690.
[2] J.Y. Chung, Y. Ahn, J.H. Lee, S. Yang, S.C. Lee, H. Kong, H.J. Chung, Microbubble-controlled delivery of biofilm-targeting nanoparticles to treat MRSA infection, Adv. Funct. Mater. 44 (2025) 2508291.
[3] B. Li, Z. Xu, R. Wang, R. Nie, Z. Tao, X. Huang, Mineralizing biofilm towards sustainable conversion of plastic wastes to hydrogen, Angew. Chem. Int. Ed. 64 (2025) e202416577.
[4] A. Nabawy, A.N. Chattopadhyay, J.M.V. Makabenta, M.A. Hassan, J. Yang, J. Park, M. Jiang, T. Jeon, J. Im, V.M. Rotello, Cationic conjugated polymers with tunable hydrophobicity for efficient treatment of multidrug-resistant wound biofilm infections, Biomaterials 316 (2025) 123015.
[5] H. Liu, T. Wu, Y. Xin, W. Wang, D. Sun, M. Su, Y. Yu, J. Zhao, M. Elsabahy, H. Gao, Targeted eradication of fusobacterium nucleatum biofilms to reverse tumor immunosuppression and inhibit E-cadherin/β-catenin signaling for colorectal cancer therapy, Chem. Eng. J. 534 (2026) 175111.
[6] X. Han, Q. Lou, F. Feng, G. Xu, S. Hong, L. Yao, S. Qin, D. Wu, X. Ouyang, Z. Zhang, X. Wang, Spatiotemporal release of reactive oxygen species and NO for overcoming biofilm heterogeneity, Angew. Chem. Int. Ed. 61 (2022) e202202559.
[7] L. Shi, C. Xue, X. Zhao, Y. Wang, Q. Shuai, Self-propelled galactose- targeted nanomotors enabling synergistic photothermal/gas therapy for antibiotic-free eradication of Pseudomonas aeruginosa biofilms, Chem. Eng. J. 529 (2026) 172989.
[8] G. Batoni, L. Martinez-Pomares, S. Esin, Editorial: immune response to biofilms, Front. Immunol. 12 (2021) 696356.
[9] A. Thakur, R. Ganesan, J. Ray Dutta, Breaching the biofilm fortress: overcoming microbial resuscitation in a de novo bacterial strain through synergistic cellulase–antibiotic action, Chem. Eng. J. 531 (2026) 174113.
[10] M.D.M. Cendra, E. Torrents, Pseudomonas aeruginosa biofilms and their partners in crime, Biotechnol. Adv. 49 (2021) 107734.
[11] J. Ma, Z. Teng, L. Ding, X. Peng, Y. Xie, Q. Long, L. Jiang, S. Huo, X. Liang, G. Liu, Ultrasound-triggered nano-bomb: bacteria-targeted oxygen-supplying liposomes as seed bubbles for enhanced mechano-sonodynamic therapy of *Pseudomonas aeruginosa* biofilms, Adv. Funct. Mater. 41 (2025) 2501347.
[12] C. Werlang, G. Cárcarmo-Oyarce, K. Ribbeck, Engineering mucus to study and influence the microbiome, Nat. Rev. Mater. 4 (2019) 134.
[13] C.A. Werlang, J.K. Sahoo, G. Carcarmo-Oyarce, C. Stevens, D. Uzun, R. Putnik, O. Hasturk, J. Choi, D.L. Kaplan, K. Ribbeck, Selective biofilm inhibition through mucin-inspired engineering of silk Glycopolymers, J. Am. Chem. Soc. 146 (2024) 34661.
[14] R. Joseph, A. Naugolny, M. Feldman, I.M. Herzog, M. Fridman, Y. Cohen, Cationic Pillararenes potently inhibit biofilm formation without affecting bacterial growth and viability, J. Am. Chem. Soc. 138 (2016) 754.
[15] Z. Han, Y. Xu, H. Gu, T. Zhang, D. Ren, Biofilm control by active topography with mucin coating, Adv. Funct. Mater. 35 (2025) 2422753.
[16] N.Y. Kruchinin, M.G. Kucherenko, Conformational changes of a complex of two oppositely charged polyelectrolytes on the surface of a polarized spherical metal nanoparticle, Chin. J. Chem. Eng. 85 (2025) 25.

[17] X. Zhang, Y. Li, R. Zhang, Y. Chen, G. Zhao, W. Zhao, X.-C. Chen, S. Zhang, Reversible visualization from exponentially growing polyelectrolyte assemblies with regionally confined dynamic structures, Chem. Eng. J. 425 (2021) 131445.
[18] X.C. Chen, K.F. Ren, J.H. Zhang, D.D. Li, E. Zhao, Z.J. Zhao, Z.K. Xu, J. Ji, Humidity-triggered self-healing of microporous polyelectrolyte multilayer coatings for hydrophobic drug delivery, Adv. Funct. Mater. 25 (2015) 7470.
[19] S. Sant, D.F. Coutinho, A.K. Gaharwar, N.M. Neves, R.L. Reis, M.E. Gomes, A. Khademhosseini, Self-assembled hydrogel fiber bundles from oppositely charged polyelectrolytes mimic micro-/nanoscale hierarchy of collagen, Adv. Funct. Mater. 27 (2017) 1606273.
[20] R. Zhao, B. Tang, Z. Xu, G. Fang, β-Cyclodextrin-based polyelectrolyte complexes for drug delivery, Coord. Chem. Rev. 534 (2025) 216581.
[21] M. Fu, C. Luo, Q. Yuan, Z. Ma, Q. Long, B. Liu, D. Wu, J. Xu, X. Li, Bifunctional reduced graphene oxide/polyelectrolytes/MoS_2-AuNPs hybrids with Vis/NIR photocatalytic and photothermal activities for biosafe and efficient antibacterial applications, J. Environ. Chem. Eng. 12 (2024) 114779.
[22] J.A. Finbloom, P. Raghavan, M. Kwon, B.N. Kharbikar, M.A. Yu, T.A. Desai, Codelivery of synergistic antimicrobials with polyelectrolyte nanocomplexes to treat bacterial biofilms and lung infections, Sci. Adv. 9 (2023) eade8039.
[23] B.C. Borro, M. Malmsten, Complexation between antimicrobial peptides and polyelectrolytes, Adv. Colloid Interf. Sci. 270 (2019) 251.
[24] C. Shen, L. Xu, G. Zhang, Q. Meng, Layer-by-layer self-assembly of core/shell pH-responsive MOF microcarriers coated with polyelectrolyte hydrogels for controlled antimicrobial delivery, Chem. Eng. J. 524 (2025) 169139.
[25] X. Zhu, C. Wei, H. Chen, C. Zhang, H. Peng, D. Wang, J. Yuan, J.H. Waite, Q. Zhao, A cation-methylene-phenyl sequence encodes programmable poly(ionic liquid) coacervation and robust underwater adhesion, Adv. Funct. Mater. 32 (2021) 2105464.
[26] A.B. Marciel, E.J. Chung, B.K. Brettmann, L. Leon, Bulk and nanoscale polypeptide based polyelectrolyte complexes, Adv. Colloid Interf. Sci. 239 (2017) 187.
[27] J. Akintola, Y. Chen, Z.A. Digby, J.B. Schlenoff, Antifouling coatings from glassy polyelectrolyte complex films, ACS Appl. Mater. Interfaces 15 (2023) 50058.
[28] D. Cui, A. Szarpak, I. Pignot-Paintrand, A. Varrot, T. Boudou, C. Detrembleur, C. Jérôme, C. Picart, R. Auzély-Velty, Contact-killing polyelectrolyte microcapsules based on chitosan derivatives, Adv. Funct. Mater. 20 (2010) 3303.
[29] B.P. Das, M. Tsianou, From polyelectrolyte complexes to polyelectrolyte multilayers: electrostatic assembly, nanostructure, dynamics, and functional properties, Adv. Colloid Interf. Sci. 244 (2017) 71.
[30] I.A. Ramírez Marrero, S.L. Perry, Fundamentals and design rules of polyelectrolyte complex materials: a comprehensive review, Chem. Rev. 126 (2026) 5413–5443.
[31] A.R. Cruz, M.A.d. Boer, J. Strasser, S.A. Zwarthoff, F.J. Beurskens, C.J.C. de Haas, P.C. Aerts, G. Wang, R.N. de Jong, F. Bagnoli, J.A.G. van Strijp, K.P.M. van Kessel, J. Schuurman, J. Preiner, A.J.R. Heck, S.H.M. Rooijakkers, Staphylococcal protein A inhibits complement activation by interfering with IgG hexamer formation, Proc. Natl. Acad. Sci. USA 118 (2021) e2016772118.
[32] V. Amritkar, S. Adat, V. Tejwani, A. Rathore, R. Bhambure, Engineering staphylococcal protein a for high-throughput affinity purification of monoclonal antibodies, Biotechnol. Adv. 44 (2020) 107632.
[33] Y. Xu, D. Tang, L. Li, X. Li, Q. Chang, H. Xiao, W. Li, A Bodipy-based aggregation-induced emission nanoagent for sonodynamic antibacterial studies, Adv. Funct. Mater. 34 (2024) 2315385.
[34] R. Guo, K. Li, B. Tian, C. Wang, X. Chen, X. Jiang, H. He, W. Hong, Elaboration on the architecture of pH-sensitive surface charge-adaptive micelles with enhanced penetration and bactericidal activity in biofilms, J. Nanobiotechnol. 19 (2021) 232.
[35] J. Wang, X.Y. Chen, Y. Zhao, Y. Yang, W. Wang, C. Wu, B. Yang, Z. Zhang, L. Zhang, Y. Liu, X. Du, W. Li, L. Qiu, P. Jiang, X.Z. Mou, Y.Q. Li, pH-switchable antimicrobial nanofiber networks of hydrogel eradicate biofilm and rescue stalled healing in chronic wounds, ACS Nano 13 (2019) 11686.
[36] B.Z. Cavari, Y. Avi-Dor, Effect of carbonyl cyanide m-chlorophenylhydrazone on respiration and respiration-dependent phosphorylation in *Escherichia coli*, Biochem. J. 103 (1967) 601–608.
[37] Z. Zhao, Y. Zhao, X.-Y. Zhuang, W.-C. Lo, M.A.B. Baker, C.-J. Lo, F. Bai, Frequent pauses in Escherichia coli flagella elongation revealed by single cell real-time fluorescence imaging, Nat. Commun. 9 (2018) 1885.
[38] X. Li, L. Lei, J. Yu, X. Wu, W. Hu, H. Lin, Emerging risk of chronic microplastic exposure: evolution of Escherichia coli toward antibiotic resistance and pathogenicity, Chem. Eng. J. 523 (2025) 168621.
[39] N. Wadhwa, H.C. Berg, Bacterial motility: machinery and mechanisms, Nat. Rev. Microbiol. 20 (2021) 161.
[40] V. Lagage, S. Uphoff, Filming flagella and pili in action, Nat. Rev. Microbiol. 16 (2018) 584.
[41] L. Wang, Q. Cai, Y. Yang, Q. Mai, Y. Zhou, Y. Liu, Y. Liu, J. Liu, Reshaping bacterial microenvironments: hybrid biomimetic membrane-coated copper nanosystems combat bacterial biofilm infections by inhibiting bacterial quorum sensing systems, Chem. Eng. J. 512 (2025) 162088.
[42] W. Xiu, X. Li, Q. Li, M. Ding, Y. Zhang, L. Wan, S. Wang, Y. Gao, Y. Mou, L. Wang, H. Dong, Ultrasound-stimulated “exocytosis” by cell-like microbubbles enhances antibacterial species penetration and immune activation against implant infection, Adv. Sci. 11 (2024) 2307048.
[43] X. Li, Q. Li, A. He, M. Dang, Y. Zhang, M. Wang, Q. Sun, Z. Dai, M. Ding, J. Zheng, Y. Mou, W. Xiu, H. Dong, Disrupting biofilm tolerance by ionic microbubble-mediated copper ion surge for infection clearance, ACS Nano 19 (2025) 28624–28643.
[44] A. Harms, E. Maisonneuve, K. Gerdes, Mechanisms of bacterial persistence during stress and antibiotic exposure, Science 354 (2016) aaf4268.
[45] Z. Wang, P. Zhang, C. Yin, Y. Li, Z. Liao, C. Yang, H. Liu, W. Wang, C. Fan, D. Sun, L. Cheng, Antibiotic-derived carbon-nanodot-decorated hydrogel for reactive oxygen species-enhanced anti-infection through biofilm damage, Adv. Funct. Mater. 33 (2023) 2300341.
[46] X. Xia, W. Huang, Z. Wei, F. Fang, L. Su, J. Luo, Y. Wu, Selective enrichment of gram-staining bacteria by antimicrobial pressure enhances volatile fatty acids production from waste activated sludge, Chem. Eng. J. 514 (2025) 163307.